

The effect of a small magnetic flux on the metal-insulator transition

Lukas Jahnke,¹ Jan W. Kantelhardt,¹ and Richard Berkovits²

¹*Institut für Physik, Martin-Luther-Universität Halle-Wittenberg, 06099 Halle, Germany*

²*Minerva Center and Department of Physics, Bar-Ilan University, Ramat-Gan 52900, Israel*

(Dated: 28.1.2009, version 1.0)

We numerically show that very small magnetic flux can significantly shift the metal-insulator transition point in a disordered electronic system. The shift we observe for the 3d Anderson model obeys a power law as predicted by Larkin and Khmel'nitskii (1981). We compute the exponent and find good agreement with the prediction. However, the power law holds only for much smaller magnetic fields than has been previously assumed, and is accompanied by a large prefactor, leading to a surprising strong dependence of the transition point on the applied magnetic field. Furthermore, we show that the critical level-spacing distribution is identical in the presence and absence of a magnetic field if hard-wall boundary conditions are applied. This result is surprising since both cases belong to different universality classes and different distributions have been reported for periodic boundary conditions.

PACS numbers: 71.30.+h, 75.47.-m, 72.15.Rn

I. INTRODUCTION

The interest in measuring small magnetic fields is driven by the possibility to build smaller magnetic storage devices with high capacity. Much progress in the understanding of the magnetic properties of condensed matter has been achieved in the last decades especially in thin layers¹. Some of the results were honored by a Nobel price in physics in 2007 for the discovery of the giant magneto resistance by Fert and Grünberg.

In this paper we want to take a different path, studying the influence of a magnetic field on a metal-insulator transition (Anderson transition)² rather than on the magnetization. Already in the eighties, Larkin and Khmel'nitskii³ estimated the shift of the metal-insulator transition point, i.e., the critical disorder W_c for small magnetic fluxes ϕ as

$$W_c(\phi) - W_c(0) = \Delta\phi^{\beta/\nu} \quad \text{with } \beta = 1/2 \quad (1)$$

and ν the scaling exponent of the localization length, $\lambda(W) \sim (W - W_c)^{-\nu}$. The value $\nu \approx 1.43$ was numerically calculated for large and random magnetic fluxes in 3D cubic lattices⁴. The prediction (1) was verified with different sophisticated analytical studies^{5,6,7,8,9,10,11}. On the other hand, numerical work concentrated on the effect of large or random magnetic fluxes⁴. Computation of the shift of the mobility edge as function of the magnetic field shift was performed only once¹², with large error bars and for relatively large fluxes. However, since Eq. (1) should be correct only for small fluxes a more thorough numerical analysis is needed.

Here we show that for small magnetic fluxes the shift of the critical disorder W_c is a power law following Eq. (1) very closely. Deviations occur for $\phi > 0.03$, in particular for the ϕ values previously considered¹². Moreover, our numerical results show a surprisingly large prefactor Δ in Eq. (1), which leads to a very large shift even for small values of ϕ . Basically, half of the total shift in W_c takes place for fluxes which are more than hundred times

smaller than the ones previously considered. This could possibly be exploited for devices detecting small magnetic fields. Various experiments have demonstrated the possibility to reproduce properties seen in the Anderson model including effects of magnetic fields^{13,14,15}.

In addition to the shift of the critical disorder W_c induced by $\phi > 0$ a change in the critical level-spacing distribution with magnetic field was reported¹⁶. These results were obtained with periodic boundary conditions. On the other hand, it is known that a change of boundary conditions also changes the critical level-spacing distribution^{17,18}. Here we show that for hard-wall boundary conditions one finds *identical* critical level-spacing distribution functions in the presence and absence of a magnetic flux, even though the magnetic field changes the universality class of the system. We also examine the second moment of the critical level spacing distributions and confirm its dependence on the boundary condition¹⁷. Furthermore, we examine its dependence on the magnetic flux for periodic and hard wall boundary conditions and find no changes in both cases.

The outline of the paper is as follows. In Section II we introduce the model and also describe the finite-size fitting procedures we employed to determine the critical disorders W_c . In Section III we discuss the main results presenting the phase diagram and comparing with Eq. (1). Section IV is devoted to the effect of boundary conditions on the critical level spacing distribution and its second moment. Section V gives conclusion and outlook.

II. MODEL AND FINITE-SIZE SCALING APPROACH

To study metal-insulator transitions (MIT) on a 3D simple cubic lattice we consider the tight-binding

Hamiltonian²,

$$H = \sum_i \epsilon_i a_i^\dagger a_i - \sum_{(i,j)} t_{j,i} a_j^\dagger a_i, \quad (2)$$

where the first part represents the disordered on-site (node) potential (homogeneous distribution $-W/2 < \epsilon_i < W/2$) and the second part describes the transfer between neighboring sites (i, j) . The transfer probability is given by $t_{i,j} = \exp(i\varphi_{i,j})$ for neighboring lattice points where $\varphi_{i,j}$ is the phase accumulation of the hopping electron. A constant magnetic field \mathbf{B} is applied by choosing phases such that the flux ϕ per plaquette (unit square) in the xy -plane is in between 8×10^{-4} and 0.25 in units of the flux quantum $\varphi_0 = hc/e$. The lowest value is derived from the smallest system size $L/a = 14$ we consider here, with a the lattice constant defining the length scale. For lower fluxes the magnetic length $L_H/a = 1/(\sqrt{2\pi\phi})$ would become smaller than L , and the electrons will not accumulate a 2π phase shift. The largest flux we consider is given by the symmetry of the problem¹⁹. The relation between the flux per plaquette and a given magnetic field depends on the lattice constant a , $\phi = eBa^2/h$. We choose hard wall boundary conditions in most calculations to avoid discontinuities in the phase accumulation of the hopping electrons due to the magnetic field.

To calculate the eigenvalues of 3D systems with the Hamiltonian (2) we use an iterative solver based on a general Davidson and Olsen algorithm²³ where the matrix vector multiplication is performed by *Intel MKL Pardiso*. We calculate six eigenvalues around $|E| = 0$ for each configuration with linear system sizes ranging from $L/a = 14$ to $L/a = 40$ lattice points, accumulating at least 2×10^5 eigenvalues for each size.

It is expected that a second-order phase transition occurs for a given critical disorder W_c . For an infinite system this transition is characterized by the divergence of the correlation length λ . The divergence is described by $\lambda(W) \sim (W - W_c)^{-\nu}$ with a critical exponent ν . We study this transition by analyzing the level-spacing distribution $P(s)$ of consecutive eigenvalues E_i , with $s = (E_i - E_{i-1})/\Delta E$ and the mean level spacing ΔE .

In the limit of infinite system size the level-spacing distribution $P(s)$ of a disordered system corresponds to a random-matrix theory result if the eigenfunctions are extended. For systems which obey time-reversal symmetry the corresponding random-matrix ensemble is the orthogonal Gaussian ensembles (GOE), well approximated by the Wigner surmise, $P_{\text{GOE}}(s) = (\pi/2)s \exp(-\pi s^2/4)$ (dashed red line in Fig. 1). A magnetic field breaks the time reversal symmetry, changing the ensemble to a unitary Gaussian ensemble (GUE), for which the level-spacing distribution is approximated by $P_{\text{GUE}}(s) = (32/\pi^2)s^2 \exp(-4s^2/\pi)$ (dotted red line in Fig. 1). In contrast to the metallic phase, the uncorrelated energy levels of localized states are characterized by a Poisson distribution, $P_{\text{P}}(s) = \exp(-s)$ (dashed dotted purple line in Fig. 1), independent of the symmetry.

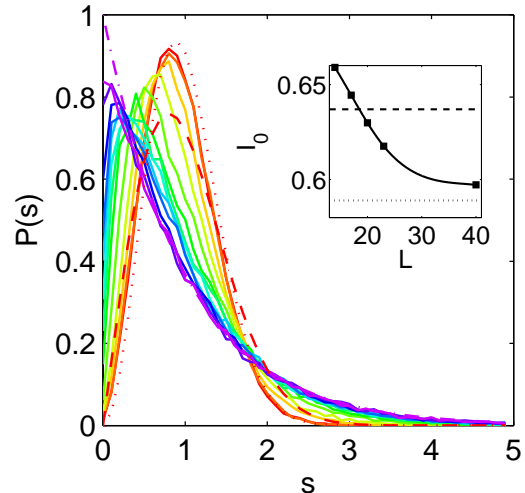


FIG. 1: (Color online) The level spacing distribution $P(s)$ for a system of size $L/a = 40$ and magnetic flux per plaquette $\phi = 10^{-3}$. In the metallic phase (red curves) the level spacing follows the GUE distribution (dotted red curve) rather than the GOE distribution (dashed red curve). A clear transition from GUE to Poisson (dash-dotted purple curve) behavior is observed as the disorder increases from $W = 8$ (continuous red curve) to $W = 23$ (continuous purple curve). Inset: System size dependence of $I_0 = \langle s^2 \rangle / 2$ for $W = 10$. With increasing system size the GUE value (dotted line) is clearly reached asymptotically rather than the GOE value (dashed line).

For finite systems $P(s)$ is between P_{GOE} (or P_{GUE} with a magnetic field) and $P_{\text{P}}(s)$. However, it approaches one of them with increasing system size, remaining system-size independent only at the transition point, i.e. for $W = W_c$. To determine the critical disorder we study the system-size (L) dependence, of the second moment of the level spacings, $I_0 = \langle s^2 \rangle / 2$. From one-parameter finite-size scaling arguments^{20,21} we expect that I_0 will depend on disorder W and lattice size L if $W \neq W_c$, but become independent of L at $W = W_c$. The second moments of a Poissonian, GOE or GUE distribution can be calculated via $\int_0^\infty s^2 P(s)$, yielding $I_{0,\text{P}} = 1$, $I_{0,\text{GOE}} = 0.637$ (dashed line in the inset of Fig. 1) and $I_{0,\text{GUE}} = 0.589$ (dotted line in the inset of Fig. 1).

Since we choose hard boundary conditions we need to take care of finite-size corrections due to irrelevant surface effects²². Therefore we fit our data to a scaling form including these irrelevant surface effects decaying with system size as a power law, $I_0 = F(\Psi L^{1/\nu}, \Xi L^y)$ with the critical exponent ν , the relevant scaling variable Ψ , the leading irrelevant variable Ξ and the leading irrelevant exponent y . For finite system sizes L no phase transition takes place and F is a smooth analytical function. After expanding F to first order one gets:

$$I_0(\phi, W, L) = F_0(\Psi L^{1/\nu}) + \Xi L^y F_1(\Psi L^{1/\nu}). \quad (3)$$

where F_0 and F_1 are analytical functions and are ex-

panded to third order in the analysis of the numerical results. The relevant and irrelevant scaling variables are expanded in power series of the dimensionless disorder $w = (W_c - W)/W_c$. The relevant variable is expanded to first order, $\Psi(w) = \Psi_1(W_c - W)/W_c$, whereas we expand to zeroth order the irrelevant variable, $\Xi(w) = \Xi_0$. In total there are eleven independent fit parameters with W_c and ν being the interesting ones (see Ref.²² for the details of the procedure).

Figure 1 shows the level-spacing distributions of a system of size $L/a = 40$ and magnetic flux $\phi = 10^{-3}$ per plaquette. A transition can be observed from a metallic phase, where the level-spacing distribution is close to GUE, for $W = 8$ (continuous red line), to an insulating phase with $P(s)$ close to Poisson, for $W = 23$ (continuous purple line). When comparing the continuous red line with the dotted red curve, a clear similarity can be observed. This means that the metallic state is similar to a random matrix GUE ($P_{\text{GUE}}(s)$) and not GOE ($P_{\text{GOE}}(s)$). We do not observe a smooth crossover between GOE and GUE for linear system sizes larger than L_H . The same asymptotic behavior can also be seen in the size dependence of the second moment of the level spacings I_0 for a metallic state. For large system sizes and low disorder ($W = 10$), I_0 reaches the GUE value asymptotically as depicted in the inset of Fig. 1. The critical (system-size independent) level-spacing distribution occurs at $W_c \approx 17$ (continuous light blue line). This distribution will be discussed in more detail in Section IV.

Since the actual form of the critical level-spacing distribution is not known we study I_0 to extract the critical disorder values W_c and the corresponding $I_{0,c}$. In the procedure we fit our results of I_0 to Eq. (3) using a least-square method, i.e., a state of the art non-linear least-square fitting algorithm implemented in *Mathematica*. To achieve better accuracy we do not fit the results for each flux ϕ separately but simultaneously calculate a non-linear fit over certain ranges of fluxes. Such an approach is possible since W_c is the only parameter in Eq. (3) changing significantly with ϕ for small values of ϕ . To check the stability of the fits we compare several fits over different ranges of flux between $\phi = 8 \times 10^{-4}$ and $\phi = 3 \times 10^{-2}$. For large flux ($\phi = 0.1$ and 0.25) as well as for no flux ($\phi = 0$) we perform separate fits, since other parameters than W_c (in particular ν) change for the GOE ensemble ($\phi = 0$) and for large ϕ .

Figure 2(a) shows results of such a non-linear fit for $\phi = 10^{-3}$ together with the simulation results for four system sizes ($L/a = 14, 20, 30, 40$). As expected and already indicated in the inset of Fig. 1, I_0 drops with increasing system sizes reaching towards $I_{0,\text{GUE}}$ for large system sizes if $W < W_c$. For $W > W_c$, on the other hand, I_0 increases with system sizes towards $I_{0,\text{P}}$. At the critical disorder W_c , I_0 is system-size independent. The lines are the result of the simultaneous fit. Although it seems that all lines cross at $W \approx 16.8$ this is not the case as can be seen in the inset. This is due to the non-relevant

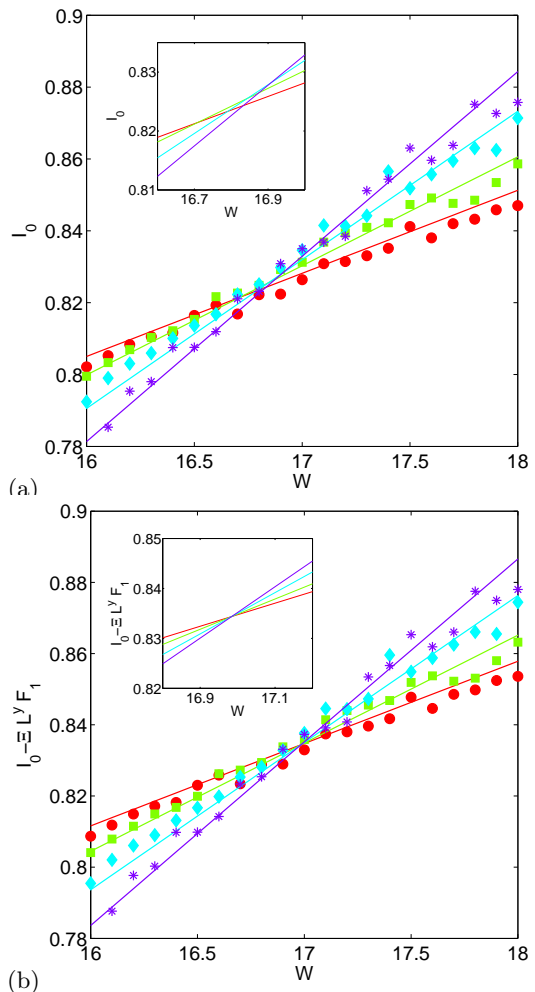


FIG. 2: (Color online) The localization parameter $I_0 = \langle s^2 \rangle / 2$ versus disorder W for system sizes $L/a = 14$ (red circles), $L/a = 20$ (green squares), $L/a = 30$ (light blue diamonds), and $L/a = 40$ (blue stars) where a magnetic flux of $\phi = 10^{-3}$ is applied. The lines correspond to fits of Eq. (3). (a) The symbols correspond to I_0 . A transition from extended states for small W to localized ones for large W is seen for all sample sizes. Nevertheless, the critical crossing point cannot be observed directly due to finite size effects. Inset: the region around $W = 16.8$ zoomed in; there is no single crosspoint. (b) Corrected values of I_0 where the influence of the irrelevant variables is subtracted. A clear transition can be seen at $W_c \approx 17$; all lines cross at one distinct critical disorder.

variables $\Xi^y F_1$ scaling with system size L . Figure 2(b) shows that subtracting the non-relevant variables leads to a nice crossover for $W_c \approx 17$ indicating a system-size independent critical value of $I_{0,c} \approx 0.83$. Taking the whole range of fluxes it is possible to draw a phase diagram of fluxes and critical disorders.

TABLE I: Result of single fits for the interesting parameters.

ϕ	0	0.1	0.25
W_c	16.59	18.21	18.30
ν	1.54	1.42	1.49
$I_{0,c}$	0.83	0.83	0.81

III. PHASE DIAGRAM AND SCALING BEHAVIOR OF THE TRANSITION

We have performed extensive numerical simulations for the entire range of magnetic fluxes¹⁹ from $\phi = 0$ to 0.25. The data is analyzed according to the description given in the previous section. The results for the extreme cases, $\phi = 0, 0.1$, and 0.25, are presented in Tab. I. For $\phi = 0$ we retrieve the well-known GOE values for W_c and ν^{22} . For $\phi = 0.1$ and $\phi = 0.25$ we also reproduce previous results^{4,12}. Interestingly, the critical value $I_{0,c}$ does not change upon applying the flux, which is also in agreement with previous work considering periodic boundary conditions^{4,12,17}.

Figure 3 summarizes our results for small fluxes, $\phi = 8 \times 10^{-4}, 10^{-3}, 1.5 \times 10^{-3}, 2 \times 10^{-3}, 4 \times 10^{-3}, 7 \times 10^{-3}, 10^{-2}$, and 3×10^{-2} , based on a simultaneous fit. The dashed line marks the flux where the magnetic length $L_H/a = \frac{1}{\sqrt{2\pi\phi}}$ coincides with our smallest system size $L/a = 14$. The values of the most important parameters W_c , ν and I_{0c} are also reported in Tab. II. They are means of the results achieved from different starting values in the fitting procedure; the errors are the absolute deviations from the means. The result for the critical exponent at small fluxes $\nu = 1.41$ is slightly lower but within the error bar range of a previous numerical study⁴ ($\nu = 1.43 \pm 0.04$). This result is similar to our results for larger fluxes ($\phi = 0.1$ and 0.25).

Our main goal, however, is to study the dependence of the critical disorder W_c on ϕ . Since the fitting approach does not use ϕ as a fitting parameter, the power-law behavior shown in Fig. 3 confirms the prediction (1) by Larkin and Khmel'nitskii³ discussed in the introduction. Although the individual error bars for $W_c(\phi)$ are still significantly large, the power-law behavior for $W_c(\phi)$ comes out naturally, even though Eq. (1) is not used in our scaling approach. The calculated exponent $\beta = 0.49 \pm 0.08$ is in perfect agreement with the predicted exponent $\beta = 1/2$.^{3,5,6,7,8,9,10,11} The error bar represents the deviations we get in the exponent when fitting the different results of $W_c(\phi)$ for the different initial fit variables. When different regimes of ϕ are used for the simultaneous fit, all $W_c(\phi)$ values shift slightly in some direction, but β stays the same. Therefore β is more exact than the error bars in Fig. 3 might indicate.

The inset of Fig. 3 shows the critical disorder $W_c(\phi)$ (indicated by squares) as function of ϕ . The red line is the same power-law fit as in the main panel. Although the

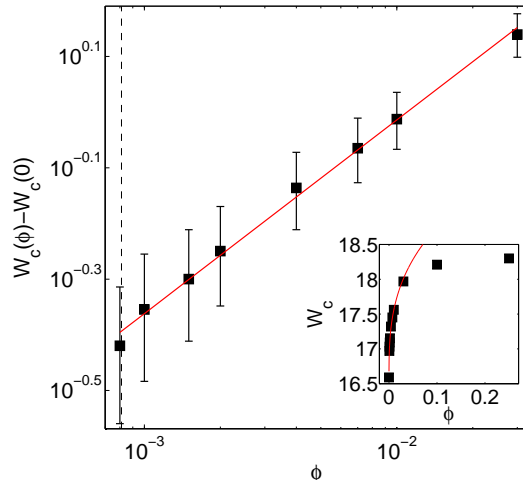


FIG. 3: (Color online) The shift of the critical disorder W_c as function of the applied magnetic field. The symbols correspond to the means obtained in a simultaneous non-linear fit of Eq. (3) with fluxes ϕ between 8×10^{-4} and 3×10^{-2} . The error bars are the absolute deviation from the mean for different initial fitting parameters. The red line is a linear fit of Eq. (1) with $\Delta = 1.57$ and $\beta/\nu = 0.35$. Hence for $\langle \nu \rangle = 1.41$ we find $\beta = 0.49$ in perfect agreement with the predicted value $\beta = 1/2$.^{3,5,6,7,8,9,10,11} Inset: The critical disorder W_c as function of ϕ for larger values of the magnetic flux. The squares correspond to the values of $W_c(\phi)$ depicted in Tab. I and II. The red line is the power law fit used in the main panel. $\phi = 0$ and $\phi = 0.25$ are symmetric axes¹⁹ and therefore the whole range of ϕ is covered. One can see the fast shift of W_c for $\phi < 3 \times 10^{-2}$, which is the region for which the scaling holds.

prediction of Larkin and Khmel'nitskii were verified it is nevertheless quite surprising how fast the critical disorder rises for small magnetic fluxes. Already at $\phi = 0.03$ most of the shift in the critical disorder has taken place. For higher magnetic fluxes ($\phi > 0.03$) the deviations from the power-law scaling are seen. We believe that such a sensitivity to small magnetic fluxes may be used as a basis for building a magnetic sensor.

IV. THE CRITICAL LEVEL SPACING DISTRIBUTION

In contrast to the critical disorder W_c the critical level-spacing distribution $P(s)$ is not universal, and it depends on the boundary conditions¹⁷. In the absence of a magnetic field¹⁷ the peak of the distribution is shifted to smaller values of s when the boundary conditions are successively changed from periodic to hard-wall in each of the three spatial directions. The tails of $P(s)$ for large s can be fitted by an exponential $P(s) \sim \exp(-\kappa s)$ with $\kappa = 1.87$ for periodic boundary conditions¹⁶ and $\kappa = 1.49$ for hard-wall (Dirichlet) boundary conditions¹⁸. The

TABLE II: Results and errors of simultaneous fit for the interesting parameters.

	$W_c(0.0008)$	$W_c(0.001)$	$W_c(0.0015)$	$W_c(0.002)$	$W_c(0.004)$	$W_c(0.007)$	$W_c(0.01)$	$W_c(0.03)$	$I_{0,c}$	ν
best fit	16.97	17.03	17.09	17.15	17.32	17.45	17.56	17.97	0.838	1.41
error	0.10	0.11	0.11	0.11	0.12	0.11	0.11	0.12	0.006	0.04

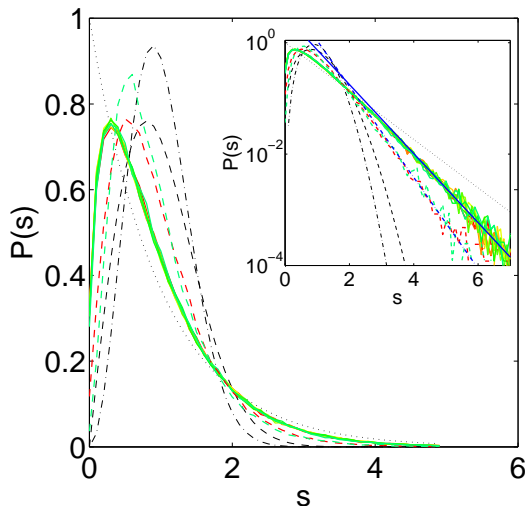


FIG. 4: (Color online) The critical level spacing distribution functions for periodic and hard-wall boundary conditions and different fluxes ϕ . For periodic boundary conditions they depend on ϕ , where the dashed red line corresponds to $\phi = 0$ and the dashed green line to $\phi = 0.1$. For hard-wall boundary conditions, there is no such dependence, as can be seen from the behavior of the continuous lines from red to green corresponding to $\phi = 0, 8 \times 10^{-4}, 10^{-3}, 1.5 \times 10^{-3}, 2 \times 10^{-3}, 4 \times 10^{-3}, 7 \times 10^{-3}, 10^{-2}, 3 \times 10^{-2}, 0.1$, and 0.25 . The limiting distributions are also shown, black dotted line – Poisson distribution, black dashed line – GOE, black dashed dotted line – GUE. Inset: a semi-log plot depicting the behavior for large s . The solid blue lines are fits to the mean tails with $\kappa = 1.42$ in the case of hard-wall boundary conditions and $\kappa = 1.88$ for periodic boundary conditions, both independent of ϕ .

critical level spacing distribution does not only change with boundary conditions but also when a magnetic flux is applied. The shape shifts towards a more GUE-like shape for periodic boundary conditions¹⁶. However, we are not aware of any numerical calculation for hard-wall boundary conditions.

Figure 4 shows the critical level-spacing distribution functions $P(s)$ for Anderson models with different magnetic fluxes ϕ and periodic as well as hard-wall boundary conditions. The results fully confirm the previous studies discussed in the previous paragraph. However, the critical level spacing distribution $P(s)$ is independent of ϕ . This new behavior of $P(S)$ for hard-wall boundary conditions is surprising, since the universality class changes from $\phi = 0$ (limit: GOE) to $\phi > 0$ (limit:

GUE) as can be seen by the different ν values (see Table I). In addition, the critical level distribution function changes when periodic boundary conditions are applied. The tails of the critical distribution confirm to the ansatz $P(s) \sim \exp(-\kappa s)$ with $\kappa = 1.88$ for periodic boundary conditions and $\kappa = 1.42$ for hard-wall boundary conditions independent of ϕ . The fits are depicted in the inset of Fig. 4.

The critical second moment $I_{0,c}$ depends also on the boundary conditions. In the literature one finds values for periodic boundary conditions, $I_{0,c} = 0.71$ ^{17,24} and for hard-wall boundary conditions $I_{0,c} = 0.81$ ¹⁷ for $\phi = 0$. We confirm both numbers numerically for $\phi = 0$ and $\phi \neq 0$. In the case of periodic boundary conditions the shape of $P(s)$ changes when a magnetic flux is introduced but the critical second moment stays the same.

V. SUMMARY AND CONCLUDING REMARKS

Our main goal has been to confirm that the shift in the critical disorder $W_c(\phi)$ for small values of the magnetic flux ϕ follows the scaling behavior $W_c(\phi) - W_c(0) = \Delta \phi^{\beta/\nu}$ with $\beta = 1/2$ as predicted by Larkin and Khmel'nitskii³. After a careful numerical study we are able to confirm this prediction, however, the prefactor Δ is much larger than expected from previous numerical studies¹². Thus, the scaling holds only for a narrow range of small fluxes up to $\phi \approx 0.03$ resulting in the fact that very weak fluxes have a strong effect on the resistivity of a sample at low temperature. This type of behavior naturally leads to the observation that the effect might be used as the basis of an extremely sensitive low-temperature sensing device.

In addition we have further considered the effects of boundary conditions and magnetic fields on the details of the metal-insulator transition of a 3D Anderson model. The results could be summarized as follows: the critical disorder W_c is independent of the boundary conditions although it depends on ϕ . The opposite is true for the critical second moment $I_{0,c}$ of the level spacing distribution $P(s)$, which is independent of ϕ but changes with boundary conditions. The flux dependence of the critical level spacing $P(s)$ is sensitive to the boundary conditions.

Acknowledgment: This work has been supported by the Minerva Foundation, the Israel Science Foundation (Grant 569/07), and the Deutsche Forschungsgemeinschaft (DFG, within SFB 418).

-
- ¹ *Handbook of Magnetism and Advanced Magnetic Materials*, edited by H. Kronmüller and S. Parkin, (John Wiley & Sons, 2007).
- ² P. W. Anderson, Phys. Rev. **109**, 1492 (1958).
- ³ D. E. Khmel'nitskii and A. I. Larkin, Solid State Commun. **39**, 1069 (1981).
- ⁴ K. Slevin and T. Ohtsuki, Phys. Rev. Lett. **78**, 4083 (1997); T. Kawarabayashi, B. Kramer, and T. Ohtsuki, Phys. Rev. B **57**, 11842 (1998); T. Ohtsuki, K. Slevin, and T. Kawarabayashi, Ann. Phys. (Leipzig) **8**, 655 (1999).
- ⁵ JY. Yuan and T. R. Kirkpatrick, J. Stat. Phys. **64**, 309 (1991).
- ⁶ M. Biafore, C. Castellani, and G. Kotliar, Nucl. Phys. B **340**, 617 (1990).
- ⁷ C. Castellani and G. Kotliar, Physica A **167**, 294 (1990).
- ⁸ F. J. Wegner, Nucl. Phys. B **270**, 1 (1996).
- ⁹ R. Oppermann, J. Phys. Lett. (Paris) **45**, 1161 (1984).
- ¹⁰ D. Belitz, Solid State Commun. **52**, 989 (1984).
- ¹¹ B. Shapiro, Philos. Mag. B **50**, 241 (1984).
- ¹² T. Dröse, M. Batsch, I. K. Zharekeshev, and B. Kramer, Phys. Rev. B **57**, 38 (1998).
- ¹³ V. F. Mitin, V. K. Dugaev, and G. G. Ihas, App. Phys. Lett. **91**, 202107 (2007).
- ¹⁴ M. Watanabe, K. M. Itoh, Y. Ootuka, and E. E. Haller, Phys. Rev. B **60**, 15818 (1999).
- ¹⁵ E. Tousson, V. Volterra, E. P. Rubenstein, R. Rosenbaum, and Z. Ovadyahu, Philos. Mag. B **56**, 875 (1987).
- ¹⁶ M. Batsch, L. Schweitzer, I. Kh. Zharekeshev, and B. Kramer, Phys. Rev. Lett. **77**, 1552 (1996).
- ¹⁷ D. Braun, G. Montambaux, and M. Pascaud, Phys. Rev. Lett. **81**, 1062 (1998).
- ¹⁸ L. Schweitzer and H. Potempa, Physica A **266**, 486 (1999).
- ¹⁹ D. R. Hofstadter, Phys. Rev. B **14**, 2239 (1976).
- ²⁰ B. I. Shklovskii, B. Shapiro, B. R. Sears, P. Lambrianides, and H. B. Shore, Phys. Rev. B **47**, 11487 (1993).
- ²¹ E. Hofstetter and M. Schreiber, Phys. Rev. B **48**, 16979 (1993); *ibid* Phys. Rev. B **49**, 14726 (1994).
- ²² K. Slevin and T. Ohtsuki, Phys. Rev. Lett. **82**, 382 (1999); K. Slevin, T. Ohtsuki, and T. Kawarabayashi, *ibid* **84**, 3915 (2000).
- ²³ A. Stathopoulos, SIAM J. Sci. Comput. **29**, 481 (2007); A. Stathopoulos and J. R. McCombs, *ibid* **29**, 2162 (2007).
- ²⁴ I. Varga, E. Hofstetter, M. Schreiber, and J. Pipek, Phys. Rev. B **52**, 7783 (1995).